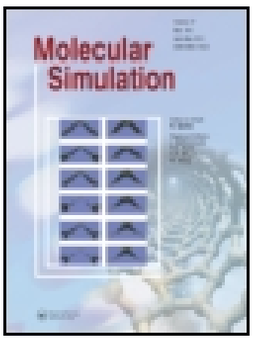

Molecular Simulation

ISSN: 0892-7022 (Print) 1029-0435 (Online) Journal homepage: https://www.tandfonline.com/loi/gmos20

Multiscale computational prediction of β-sheet peptide self-assembly morphology

Li Deng & Yanting Wang

To cite this article: Li Deng & Yanting Wang (2020): Multiscale computational prediction of β-sheet peptide self-assembly morphology, Molecular Simulation, DOI: 10.1080/08927022.2020.1738426

To link to this article: https://doi.org/10.1080/08927022.2020.1738426

MOLECULAR SIMULATION
https://doi.org/10.1080/08927022.2020.1738426

Taylor & Francis
Taylor & Francis Group

Multiscale computational prediction of β-sheet peptide self-assembly morphology

Li Deng[a,b,c] and Yanting Wang [d,e]

[a]BGI-Qingdao, Qingdao, People's Republic of China; [b]State Key Laboratory of Agricultural Genomics, Shenzhen, People's Republic of China; [c]China National GeneBank, Shenzhen, People's Republic of China; [d]CAS Key Laboratory of Theoretical Physics, Institute of Theoretical Physics, Chinese Academy of Sciences, Beijing, People's Republic of China; [e]School of Physical Sciences, University of Chinese Academy of Sciences, Beijing, People's Republic of China

ABSTRACT

Although nanostructures self-assembled by short peptides are very promising in developing novel biomaterials and nanomaterials, it is still a great challenge to design the peptide molecular structure which will self-assemble into designated nanostructures. By combining elastic theory with molecular dynamics simulations, we introduce a multiscale computational approach to predict the β-sheet morphology self-assembled by short peptides in aqueous solution only based on the molecular structure of the peptide. In our approach, the gap between the elastic model and atomistic model is bridged by the simplified model, whose parameters are determined by enhanced sampling and extensive all-atom molecular dynamics simulation results at different levels. This multiscale approach is applied to two model peptides KIIIIK (KI4K) and IIIIKK (I4K2) to test its validity. The computational results, consistent with the previous experimental observations, show that KI4K with a higher ratio of inter-sheet interaction to intra-sheet interaction tends to form tube-like morphology with a larger width, while I4K2 with a lower ratio tends to form fibril with a smaller width. This methodology is anticipated to be helpful for computer-aided design of nanostructures self-assembled by short peptides.

ARTICLE HISTORY
Received 26 December 2019
Accepted 24 February 2020

KEYWORDS
Peptide self-assembly; computer prediction; multiscale simulation

1. Introduction

Nanostructures self-assembled by biological building blocks have promising potential applications in nanotechnology for developing functional biomaterials [1–3]. Peptides are of particular interest because of the variety of their self-assembled nanostructural morphologies such as vesicles, fibrils, twisting ribbons, helical ribbons, nanotubes, and nanobelts [4–7]. It is notable that macroscopic properties of the peptide-based biomaterials are determined by morphologies and elasticity of self-assemblies at the nanoscale [8]. Many experiments were intensively conducted to investigate the rational design of peptides and self-assembly conditions for controlling the morphologies self-assembled by short peptides [9–13]. Due to the highly combinational complexity of amino acid sequences and sensitiveness of physicochemistry conditions of solutions, it would be very expensive to explore short peptide self-assembling processes for obtaining a designated morphology only through experiment. Therefore, it is in strong demand to predict the self-assembling morphology of peptides at the molecular level by computational methods.

The different hierarchical molecular structures observed in experiments provide valuable insights into intermolecular interactions in peptide self-assembly [14–16]. The hierarchical structures self-assembled by short peptides contain one common structural motif named the cross-β conformation [17,18] as well as three different peptide-peptide interfaces of intra-sheet, inter-sheet, and inter-protofilament structures [19,20]. Through tuning experimental conditions such as pH, ion strength, temperature, and agitation in a self-assembly process, the change of the hierarchical structures at the molecular level is considered to be related to morphologies of nanostructures at the nanoscale. Polymorphism of an intra-sheet structure at the atomistic level is usually observed in nanostructures of amyloid peptides [21,22], and results in the appearance of nanostructures with different morphologies at different experimental conditions, such as various pHs, agitation or quiescence [23]. The morphological transformation between these structures can also be observed in one trial [4,6,24,25]. However, the pathway of forming self-assembled morphology by underlying molecular structure is still unclear.

Due to the excessive temporal and spatial lengths of the self-assembly process, various coarse-grained models [26–28] were developed in addition to all-atom ones for investigating intermolecular interactions and dynamics of short peptides self-assembly by means of computer simulation. Consistent with experiments, the polymorphism of intra-sheet structures at the atomistic level was also found in all-atom molecular dynamics (MD) simulations combining accelerated sampling for oligomers of different short peptides [29–31]. The roles of side chains in intermolecular forces were studied by steered MD simulations and enhanced sampling simulations [32,33]. Using the sophisticated MARTINI model [34], nanostructures with different morphologies observed in experiments such as tubes, plates, and fibrils were reproduced in extensive

CONTACT Yanting Wang wangyt@itp.ac.cn Institute of Theoretical Physics, Chinese Academy of Sciences, 55 East Zhongguancun Road, P. O. Box 2735, Beijing 100190, People's Republic of China

Supplemental data for this article can be accessed at https://doi.org/10.1080/08927022.2020.1738426.

simulations (many simulations with the same control parameters conducted for different input models or initial structures), and the guiding rules of screening nanostructure propensity for all 8000 possible tripeptides were proposed [35]. So far, different sub-processes of the hierarchical structures in short peptide self-assembly can only be studied separately, and there still exist gaps between molecular modelling results at different scales.

In this work, by combining an elastic theory with multiscale molecular simulation techniques, we introduce a multiscale computational approach, as illustrated in Figure 1, to predict the morphologies self-assembled by peptides according to their molecular structure. On the basis of the balance between the energy cost of intra-sheet deformation and the energy gain of inter-sheet attraction proposed in the hierarchical peptide self-assembly model [36,37], a quantitative relation between the width of the nanostructure and the self-assembled morphology has been proposed. In our approach, the intra-sheet intermolecular interactions are first determined by combining the enhanced sampling and all-atom MD simulations. The inter-sheet intermolecular interactions are then determined in the same way. The obtained data for intermolecular interactions are finally imported into the simplified elastic model developed in our previous work [38] to establish the connection between the width and the morphology of a nanostructure. Two model peptides KI4K and I4K2 are used to validate this multiscale computational approach. Consistent with the experimental results [11], our computations show that a higher ratio of inter-sheet to intra-sheet interactions and a smaller twisting angle of KI4K lead to a self-assembled nanotube structure, rather than the nanofibril structure of I4K2. This multiscale approach can be used to computationally design the molecular structures of short peptides for developing functional materials with aimed nanostructural morphologies.

2. Methods

2.1. The hierarchical peptide self-assembly model

In the hierarchical peptide self-assembly model [36], the nanostructure formed by short peptides is treated as a laminar structure composed of cross-β sheets. The inter-sheet interaction is represented by a constant energy σ between two peptides along the side-chain direction. The intra-sheet interaction is described by the elastic energy cost for deforming a cross-β sheet with respect to its equilibrium conformation, which can be written as

$$\varepsilon_{elastic} = \frac{1}{2}k_b v^2 + \frac{1}{2}k_s t_m^2 + \frac{1}{2}k_t(n_m - n_m^{(0)})^2 \tag{1}$$

where v, t_m, and n_m are bending, splaying, and twisting deformations of the cross-β sheet with respect to its equilibrium conformation, respectively; $n_m{}^{(0)}$ is the twisting angle of a ribbon in equilibrium; k_b, k_s, and k_t are the corresponding elastic constants. Equation (1) can be further refined by considering the twisted stack-like geometry of the fibril to obtain the expression for the elastic energy of the jth cross-β sheet in the nanostructure, written as

$$\begin{aligned} \varepsilon_{elastic}^{(j)} &= \frac{1}{2}k_b \frac{\theta^4 \rho_j^2}{(1+\theta^2\rho_j^2)^2} + \frac{1}{2}k_t\left(\frac{\theta}{1+\theta^2\rho_j^2} - \theta_0\right)^2 \\ \rho_j &= j - \frac{p+1}{2} \end{aligned} \tag{2}$$

where p is the total number of cross-β sheets in the nanostructure, θ is the twisting angle between two peptides, and θ_0 is the twisting angle of the equilibrium cross-β sheet. The detailed derivation from Equation (1) to Equation (2) can be found in Ref. [36]. Thus, the total energy of the nanostructure with p cross-β sheets is

$$\varepsilon_{total} = \sum_{j=1}^{p} \varepsilon_{elastic}^{(j)} - (p-1) \times \sigma \tag{3}$$

2.2. All-atom MD simulation

In the all-atom MD simulations, the N-terminal was capped with acetic anhydride and the C-terminal was amidated for both KI4K and I4K2. To be consistent with the experimental condition pH = 3 reported in Ref. [11], the side chains of all the lysine residues were protonated, and a corresponding

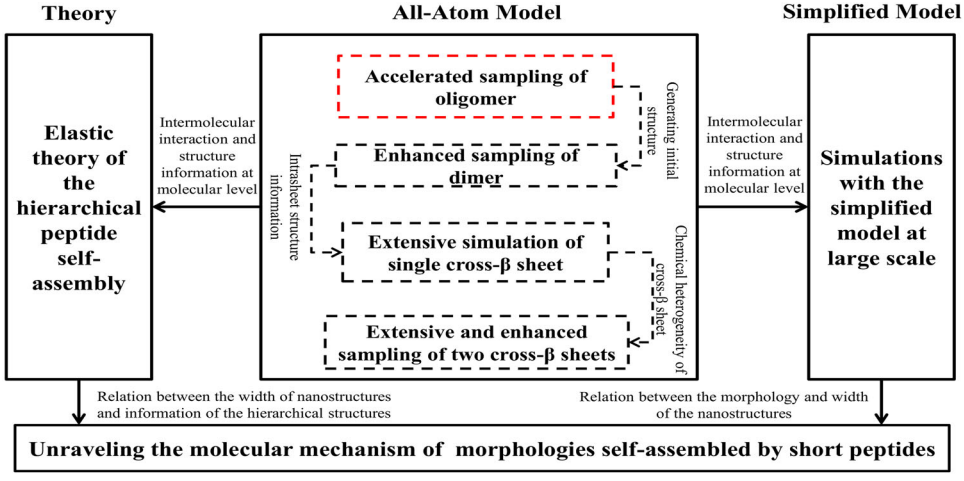

Figure 1. (Colour online) Multiscale computational approach for studying the molecular mechanism of different morphologies self-assembled by short peptides.

number of chloride ions were added to neutralise the simulated system. Both peptides and chloride ions were modelled by the OPLS-AA force field [39], and water was modelled by the TIP4P force field [40]. The initial configurations of intra-sheet structures were the most probable structures sampled by the replica exchange MD (REMD) simulation of a trimer reported in Ref. [31], while those of cross-β sheets and inter-sheet structures were manually constructed by using the Py_Mol package [41]. All-atom MD simulations with a timestep of 2 fs in a cubic box with the period boundary condition applied in three dimensions were performed in the *NPT* ensemble by using the GROMACS 4.6.5 package [42]. The cutoff for van der Waals (VDW) interactions was set to 1.2 nm. The electrostatic interactions were treated by the Particle Mesh Ewald (PME) method [43], whose cutoff in the real space was set to 1.2 nm. Chloride molecules were added to neutralise the system. The Nosé-Hoover thermostat [44] and the Parrinello-Rahman barostat [45] were used in the *NPT* ensemble simulations to control the system temperature and pressure, respectively. The stabilities of intra-sheet and inter-sheet structures were verified by conducting 50-ns simulations.

To determine the intermolecular interactions for the hierarchical structures, the rotational potential of mean force (PMF) for intra-sheet interactions and the translational PMFs for both intra-sheet and inter-sheet interactions were calculated by performing umbrella sampling simulations. For the rotational PMF for intra-sheet interactions, the reaction coordinate θ was the angle between two peptides. In these simulations, one peptide was kept fixed, and the other was rotated by using the fixed axis rotation method implemented in the enforced rotation module of GROMACS [46]. In the fixed axis rotation, the heavy atom in the fixed peptides forming the middle hydrogen bond (H-bond) between two backbones was set as the pivot point, and the vector between heavy atoms of the middle H-bond was set as the rotational axis. There were totally 90 windows ranging from 0 to 2π with a window width of 0.07 rad. and the initial configuration was selected from a 0.5-ns rotational steered MD simulation with an angular velocity of 0.174 rad/ps and a force constant of 500 kJ/mol/nm^2. Inside each window, a 10-ns *NPT* simulation with a force constant of 500 kJ/mol/nm^2 was conducted.

For the translational PMF for intra-sheet interactions, the reaction coordinate ξ was the distance between the centers-of-mass (CoMs) of peptides. There were totally 24 windows ranging from 0.44–3.0 nm with a window width of about 0.1 nm and the initial configuration was selected from a 0.5-ns SMD with a constant pulling rate of 5 nm/ns and a force constant of 1000 kJ/mol/nm^2. Inside each window, a 10-ns *NPT* simulation with a force constant of 1000 kJ/mol/nm^2 was conducted. For the translational PMF for inter-sheet interactions, the reaction coordinate ξ was the distance between the CoMs of cross-β sheets. There were totally 17 windows ranging from 1.27 to 3.0 nm with a window width of about 0.1 nm. Other simulation details were set to be the same as the translational PMF for intra-sheet interactions described above. After the umbrella sampling simulations, the weighted histogram analysis method (WHAM) [47] was used to calculate the PMFs along each reaction coordinate.

2.3. Simplified model and simulation

The simplified elastic model developed in our previous work [38] was adopted to understand the microscopic mechanism for experimentally observed morphological transformation. The energetic function of this model is

$$E = \sum_{I=1}^{N}\sum_{i=1}^{n-1}\sum_{j>i}^{n}[k_b(D_{ij}^I - D_0)^2 + k_b(R_{ij}^I - R_0)^2 + k_t(\theta_{ij}^I - \theta_0)^2] - (N-1)\times\sigma \tag{4}$$

where N is the number of cross-β sheets and n is the number of peptides in one cross-β sheet. The three terms in the square brackets describe the intra-sheet interactions between neighbouring peptides, including stretching along the H-bond direction D_{ij}^I, stretching perpendicular to the H-bond direction R_{ij}^I, and twisting degree of the cross-β sheet θ_{ij}^I, all described by harmonic potentials with D_0, R_0, and θ_0 being the equilibrium constants. The last term describes the total inter-sheet energy with the approximation that the attraction between two neighbouring cross-β sheets is a constant σ. In this model, the harmonic approximation is used to represent the intra-sheet intermolecular interactions, which provides a more direct physical view than the hierarchical peptide self-assembly model [36,37] for intermolecular interactions and allows the parameters easier to be determined from all-atom simulations.

The conformational parameters in the simplified model can be directly determined from the PMFs and all-atom MD simulation results. The twisting angle θ_0 between neighbouring peptides is the average value of twisting angles in cross-β sheets. The distance between neighbouring intra-sheet peptides D_0 and R_0 are determined from the minimal translational PMF for intra-sheet interactions. The distance between neighbouring inter-sheet peptides h_0 is determined from the minimal translational PMF for inter-sheet interactions. The twisting strength k_t is evaluated by fitting the potential well with harmonic function $\Delta G = \Delta G_0 + k_t \times (\theta - \theta_0)^2$, as shown in Figure S9, where only the intra-sheet structures feasible for width growth, as will be discussed in Section 3.4, have been fitted. Other strength parameters for intermolecular forces are evaluated based on the relations supplied by other theoretical or experimental works as well as the simulation results as follows. Because the microscopic intra-sheet interactions involved in both twisting and stretching of the intra-sheet structures mainly come from the H-bonding interactions, the stretching strength k_b was set to one half of the twisting strength k_t, as discussed in Aggeli's work [36]. In contrast to intra-sheet interactions, inter-sheet stretching comes from hydrophobic interactions, which is experimentally measured to be about one twentieth of the fibrils [19], so we set the inter-sheet energy coefficient $\sigma = (1/20)k_t\theta_0^2$ for peptides forming nanofibrils via self-assembly. For peptides forming nanostructures with different morphologies, the inter-sheet energy was determined according to the ratio between the inter-sheet translational PMFs and those of nanofibrils. The length and energy units in the simplified model are nm and k_BT, respectively, where k_B is the Boltzmann constant

and T has been set to 300 K. In all Monte Carlo (MC) simulations with the simplified model, the interval step of a trial stacking was set to 1000, the total number of steps was 10^8, and the reduced temperature was 0.01 to allow the simulation an energy minimisation procedure.

3. Results and discussions

3.1 Quantitative relation between intermolecular interactions and nanostructure width

Nanostructures self-assembled by short peptides are quite often crystal-like laminated structures of cross-β sheets [17,18]. To understand the width limit of these nanostructures in self-assembly, a classic mathematical model was proposed subject to the constraint of twisted stack-like geometry [36], where the total energy of the nanostructure with p cross-β sheets as a function of k_b, k_t, θ_0, and σ were given in Section 2.1. By minimising the total energy, the dependence of nanostructure widths on the intermolecular interactions at the microscopic level was discussed [36], which however is too complex to directly demonstrate the competition between intra-sheet and inter-sheet intermolecular interactions. Here, based on the balance between the energy cost and the energy gain of the outmost cross-β sheet, a simpler quantitative relation between the nanostructure width and intermolecular interactions will be derived as follows. With the constraint of twisted stack-like geometry, the elasticity deformation of the outmost cross-β sheet is the most significant and has the largest energy cost, which is also the driving force for the morphological transformation of nanostructures, as discussed in our previous work [38]. Considering the competition between the energy cost of intra-sheet deformation and the energy gain of inter-sheet attraction, the growth of nanostructure width will only stop when the elastic energy cost is larger than the energy gain:

$$\varepsilon_{\text{elastic}}^{(p)} \geq \sigma \tag{5}$$

The equilibrium condition is reached when the elastic energy cost of the outmost cross-β sheet is equal to the energy gain:

$$\frac{1}{2}k_b\frac{\theta^4\rho_p^2}{(1+\theta^2\rho_p^2)^2}+\frac{1}{2}k_t\left(\frac{\theta}{1+\theta^2\rho_p^2}-\theta_0\right)^2=\sigma \tag{6}$$

The general relation between the number of cross-β sheets p (proportional to the nanostructure width) and intermolecular interactions including σ, k_b, k_t, θ and θ_0 is obtained by solving Equation (6):

$$p=2\sqrt{\frac{(2k_t\theta_0-k_b\theta)+\sqrt{k_b^2\theta^2-4k_tk_b\theta_0\theta+4k_tk_b\theta_0^2+8k_t\sigma-8k_b\sigma}}{2(k_t\theta_0^2\theta-2\sigma\theta)}-\frac{1}{\theta^2}}+1 \tag{7}$$

This function is however still too complex to be practically used. To further simplify it, by considering the physical feature of peptide self-assembled structures, we assume $k_b = k_t$, namely the bending strength is the same as the twisting one, as well as $\theta = \theta_0$, namely the twisting angle of the cross-β sheet in the final state is approximately the same as the equilibrium twisting angle. Under these two approximations, we obtain a simpler relation:

$$p=\frac{2}{\theta_0\sqrt{\frac{k_t\theta_0^2}{2\sigma}-1}}+1 \tag{8}$$

In Equation (8), the nanostructure width decreases with θ_0 and k_t, but increases with σ. Furthermore, $k_t\theta_0^2/2\sigma$ inside the radical sign of the denominator describes the competition between the intra-sheet and inter-sheet interactions, which determines the nanostructure width. Usually, the inter-sheet energy gain σ originated from the interaction between side-chains cannot be larger than the intra-sheet energy cost $k_t\theta_0^2/2$ for a equilibrated twisting cross-β sheet to be untwisted, i.e. $(k_t\theta_0^2/2\sigma) > 1$, so the nanostructure morphologies are finite and twisted, e.g. twisting fibrils or twisting ribbons observed in experiments [6,37]. However, when the inter-sheet energy gain compensates the intra-sheet energy cost, namely $k_t\theta_0^2/2\sigma = 1$, the morphologies of nanostructures are infinite and flat, e.g. giant nanobelts observed in experiments [5]. The above discussion indicates the importance of intermolecular interactions at the molecular level for predicting nanostructure width.

In the following sections, the intra-sheet and inter-sheet intermolecular interactions of KI4K and I4K2 will be systematically calculated by all-atom MD simulations to explain the difference between their self-assembled morphologies.

3.2. Intermolecular interactions of intra-sheet structures

The contributions of specific residues and solvent molecules to the free energy of self-assembled nanostructures have been extensively studied by the REMD simulation method [48,49]. The REMD simulations of the trimer for both KI4K and I4K2, respectively, have unravelled the effect of charge distribution of peptides on the free energy at the microscopic level [31], but the strengths of intermolecular interactions have not been investigated. In this work, the umbrella sampling method has been used to calculate the rotational and translational PMFs of dimers along the H-bonding direction, as shown in Figure 2 (A,B,E). The rotational PMFs in Figure 2(A,B) demonstrate that there exist two minima for the KI4K dimer with both anti-parallel and parallel packing modes, but only one minimum for the I4K2 dimer with the anti-parallel packing mode. The depth of the PMF for the KI4K dimer with the anti-parallel packing mode is larger than that of the dimer with the parallel mode, and both depths of the PMFs for the KI4K dimer are smaller than that of the I4K2 dimer with the anti-parallel packing mode. The translational PMFs in Figure 2(E) demonstrate that there are no energy barriers from the dissociation state to the association state for all the intra-sheet structures, but the free energy difference between the dissociation state and the association state varies for the anti-parallel KI4K dimer (81.3 kJ/mol), the parallel KI4K dimer (52.8 kJ/mol), and the anti-

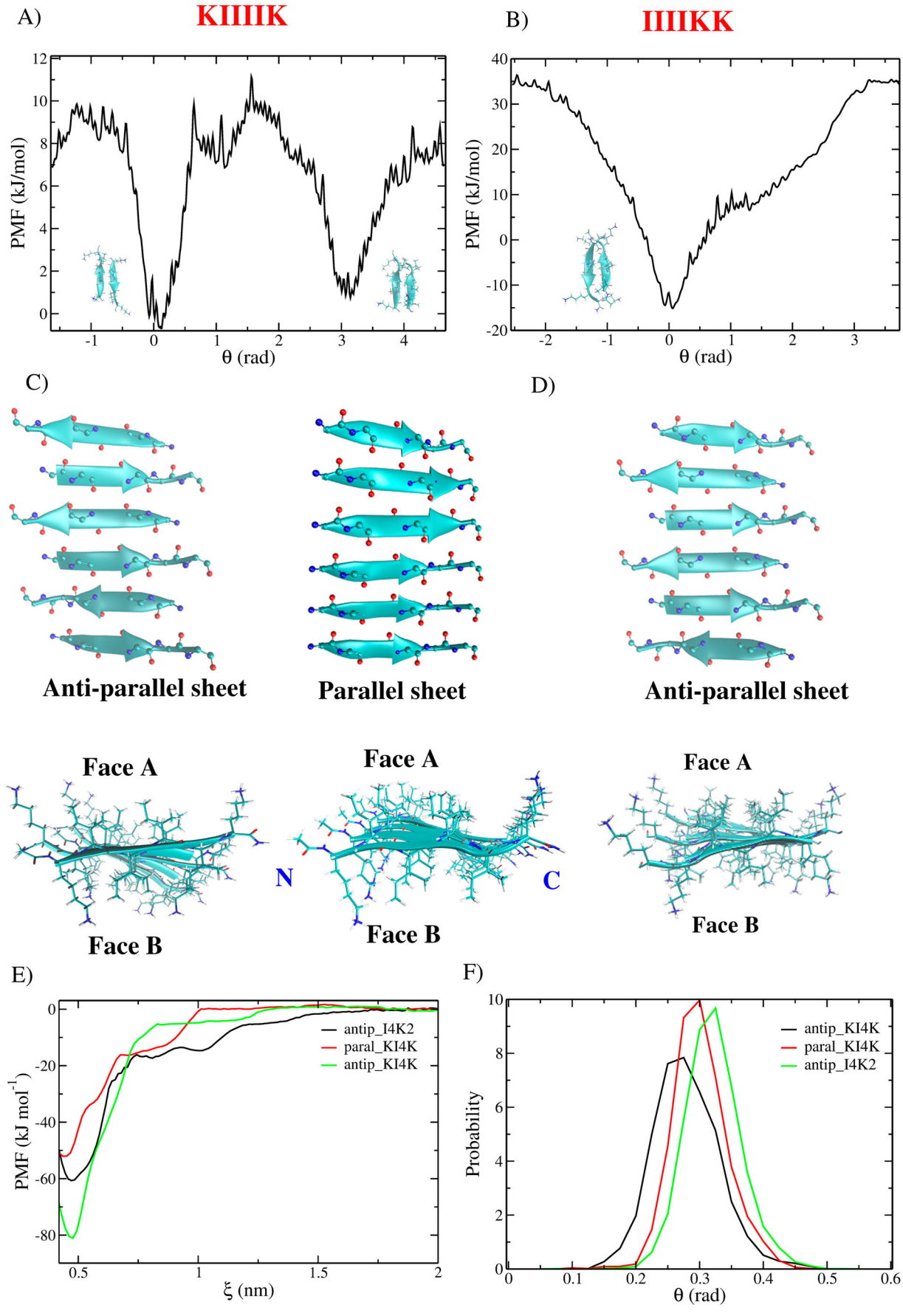

Figure 2. (Colour online) Intra-sheet interactions calculated by umbrella sampling and extensive simulations. (A) and (B) The PMFs as a function of θ for KI4 K and I4K2. (C) and (D) The cross-β sheets manually constructed according to the stable dimer structures for KI4 K and I4K2. (E) and (F) PMFs as a function of ξ for different dimers and distributions of θ for different cross-β sheets. 'N' and 'C' coloured in blue are used to distinguish the two sides of the parallel cross-β sheet.

parallel I4K2 dimer (61.2 kJ/mol). These results indicate that the distribution of charged residues in peptides can significantly affect the structures and strengths of the intermolecular interaction at the early stage of self-assembly.

Using the dimer structures with the minimal PMFs as building blocks, we can construct two kinds of cross-β sheets with six strands for KI4K, while only one is available for I4K2, as shown in Figure 2(C,D). According to the RMSD and the H-bond number shown in Figure S1, all the sheets are very stable during 50-ns MD simulations, but their physiochemical properties listed in Table 1 are different. For the anti-parallel cross-β sheets of both KI4K and I4K2, face A has larger hydrophobicity than face B and the two sides of the sheets are symmetric. For the parallel cross-β sheet of KI4K, face A is the same as face B but the two sides of the sheet are asymmetric. The intra-sheet structure can not only have effects on the physiochemical properties but also the twisting degree of the cross-β structure, as shown in Figure 2(F). The twisting degrees of both cross-β sheets of KI4K are smaller than that of I4K2, and the twisting degree of the anti-parallel cross-β sheet is smaller than that of the parallel cross-β sheet for KI4K. These results indicate that the physiochemical properties of the cross-β sheet are strongly dependent on the intra-sheet structure.

3.3 Intermolecular interactions of inter-sheet structures

Because the stability of stacking mode is essential for determining the lateral stacking structure along the side-chain direction in peptide self-assembly, all possible inter-sheet structures of KI4K and I4K2 with different stacking modes are constructed and shown in Figure S2. AtoA_antip, AtoB_antip, BtoB_antip are inter-sheet structures of two anti-parallel cross-β sheets with face A stacking to face A, face A stacking to face B, and face B stacking to face B, respectively. NC_paral and NN_paral are inter-sheet structures of two parallel cross-β sheet with side N close to side N, and side N close to side C. The face A, face B, side C, and side N are labelled in Figure 2(C,D). To compare the relative stabilities of different inter-sheet structures, the RMSD and inter-sheet distance (ISD) are calculated and shown in Figure S3, and the snapshots of inter-sheet structures at different times are shown in Figures S4 and S5. The configurations of the inter-sheet structures sampled at 45 ns are shown in Figure 3(A,B). For KI4K, the stacking modes of AtoA_antip, NtoC_paral, and NtoN_paral are stable, but the stacking direction in the NtoN_paral mode significantly deviates from the side-chain direction. For I4K2, the stacking modes of AtoA_antip and AtoB_antip are stable.

Table 1. The hydrophobic and hydrophilic areas of different faces for different cross-β sheets.

			Hydrophobic area (nm^2)	Hydrophilic area (nm^2)
KI4K	Antiparallel sheet	Face A	21.6 + 0.7	2.4 + 0.1
		Face B	18.5 + 0.6	2.4 + 0.1
	Parallel sheet	Face A	19.8 + 0.7	2.4 + 0.1
		Face B	19.3 + 0.7	2.4 + 0.1
I4K2	Antiparallel sheet	Face A	15.3 + 0.7	13.3 + 0.3
		Face B	12.4 + 0.6	13.3 + 0.3

We further verify the stability of inter-sheet structures from the thermodynamic viewpoint by calculating the PMF along the side-chain direction, and the results are shown in Figure 4. For both KI4K and I4K2, the unstable stacking modes (AtoB_antip, BtoB_antip for KI4K, and BtoB_antip for I4K2) are unfavourable in PMFs, but the stable stacking modes (AtoA_antip, NtoC_paral for KI4K, and AtoA_antip, AtoB_antip for I4K2) are favourable. The PMF differences between the association and dissociation states for all stable stacking modes of KI4K are all around −40 kJ/mol, while those of I4K2 are significantly different: −60 kJ/mol for AtoA_antip and −10 kJ/mol for AtoB_antip.

To determine the roles of hydrophobic and hydrophilic residues in stabilising the inter-sheet structures, all types of contact area of two cross-β sheets as described in the work by Chong and Ham [50], including the hydrophobic-hydrophobic-residue contacts, hydrophobic–hydrophilic-residue contacts, hydrophilic-hydrophilic-residue contacts, ant total contacts are calculated and shown in Figure 5 and Figure S6. As shown in Figure 5, the stable inter-sheet structures have larger hydrophobic contact areas than those of the unstable inter-sheet structures, demonstrating the importance of the shape complementary of hydrophobic side chains between neighbouring faces of cross-β sheets to stabilise the inter-sheet structure. The short-range energies between two sheets as a function of the distance between the CoMs of cross-β sheets are calculated and shown in Figures S7 and S8 for all kinds of inter-sheet structures of KI4K and I4K2, indicating that the VDW interactions play a crucial role in the formation of inter-sheet structures. Furthermore, these results confirm the role of the hydrophobic interaction in driving the association of cross-β sheets.

3.4. Pathway of lateral stacking for width growth

According to Figure 4, the length scales of intermolecular interaction for all stable inter-sheets are about 1.7 nm, but the CoM distances between these two sheets are about 2.4 nm. Thus, the interaction between next nearest neighbour cross-β sheets can be ignored for lateral stacking in peptide self-assembly. As shown in Figures 2(C,D) and 3, both KI4K and I4K2 have three antiparallel lateral stacking modes (AtoA_antip, AtoB_antip, and BtoB_antip), but only KI4K has two parallel lateral stacking modes (NC_paral and NN_paral). All possible ways of lateral stacking for width growth, as illustrated in Figure 6, can be constructed according to the stabilities of the inter-sheet structures. For KI4K, the PMF in Figure 4(a) indicates that AtoA_antip is the only stable antiparallel stacking mode, but because both of its outer sides are face B, it attracts neither face A nor face B, which does not allow sustainable lateral growth. Therefore, no antiparallel cross-β sheets can serve as the elemental units for building up the KI4K nanotube. On the other hand, as shown in Figure 4(a), the parallel NC_paral stacking mode is stable, and its lateral growth is sustainable, so it can serve as the elemental units for building up the KI4K nanotube. For I4K2, according to Figure 4(b), both the AtoA_antip and AtoB_antip antiparallel stacking modes are

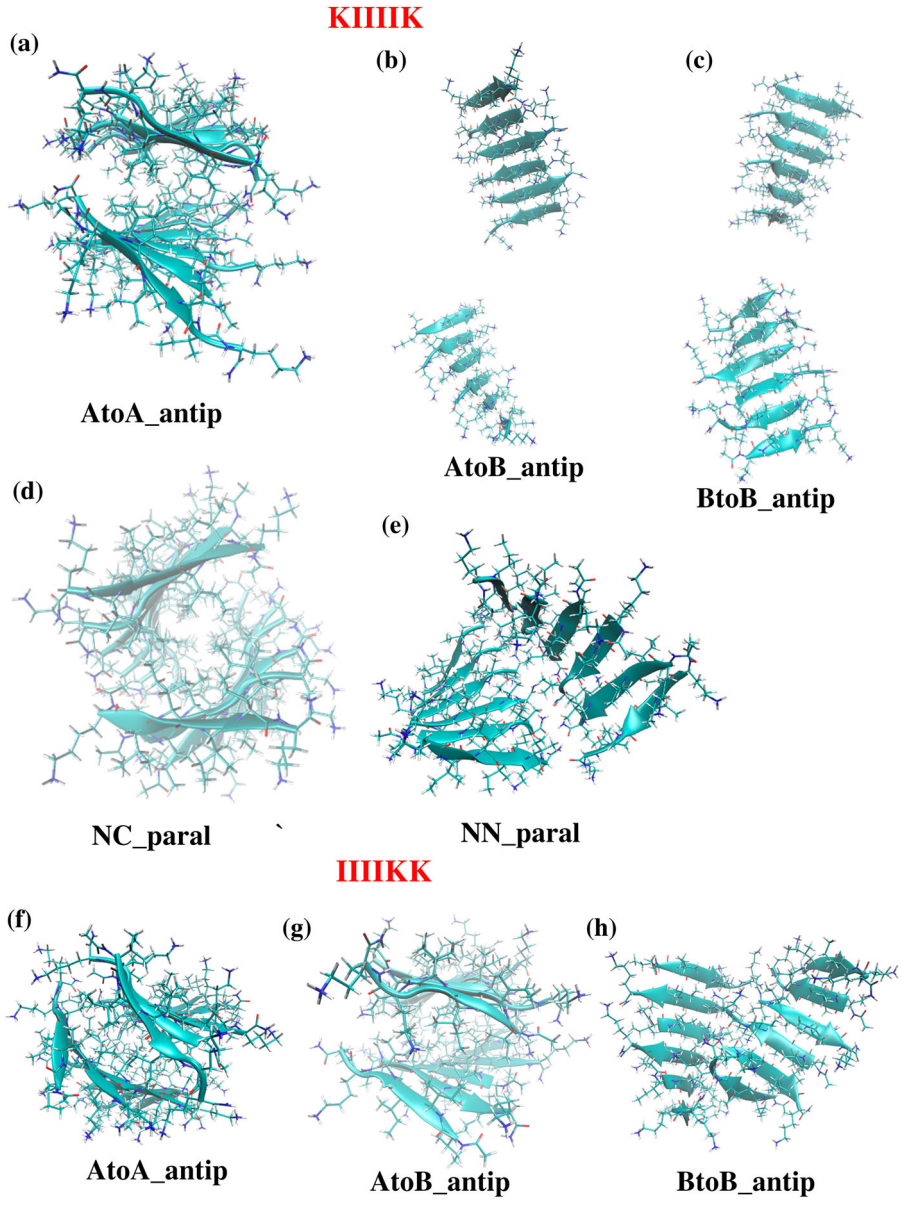

Figure 3. (Colour online) (a–e) Snapshots of all inter-sheet structures in all-atom simulations at 45 ns for KI4 K, and (f–h) snapshots for I4K2.

stable, and there exist two sustainable lateral growth pathways: one is through the mixture of AtoB_antip and only one AtoA_antip, and the other is by AtoB_antip only. Therefore, more AtoB_antip modes can be found in I4K2 fibrils than AtoA_antip modes. From the above, we can conclude that the most probable ways of forming a nanostructure with many cross-β sheets are the NtoC_paral stacking mode for KI4K and the AtoB_antip stacking mode for I4K2, respectively.

From the above all-atom MD simulations, we know that the average twisting angle of a parallel cross-β sheet in KI4K is about 0.29 rad, smaller than that of an antiparallel cross-β sheet in I4K2, which is about 0.32 rad. The depth of the potential well of the rotational PMF for the parallel cross-β sheet of KI4K is about 10 kJ/mol smaller than that for the antiparallel cross-β sheet of I4K2, which is about 45 kJ/mol. The depth of the potential well of the translational PMF for the parallel cross-β sheet of KI4K is about 52.8 kJ/mol, similar to that for the antiparallel cross-β sheet of I4K2, which is about 61.2 kJ/mol. The depth of the potential well of the translational PMF for the NtoC_paral stacking mode of KI4K is about 40 kJ/mol, larger than that for the AtoB_antip stacking mode of I4K2, which is about 10 kJ/mol. According to Equation (8), the KI4K nanostructure width should be larger than I4K2.

3.5. Morphologies of nanostructures by the simplified model

The simplified elastic model of Equation (4) developed in our previous work [38] was used through MC simulations to study the morphological transformation of nanostructures self-assembled by peptides. All the parameters acquired in the simplified model for KI4K (the parallel intra-sheet and NC_paral inter-sheet structures) and I4K2 (the antiparallel intra-sheet and AtoB_antip inter-sheet structures) are listed in Table 2, where only the energetically favourable lateral stacking modes discussed in Section 3.4 are considered. The twisting

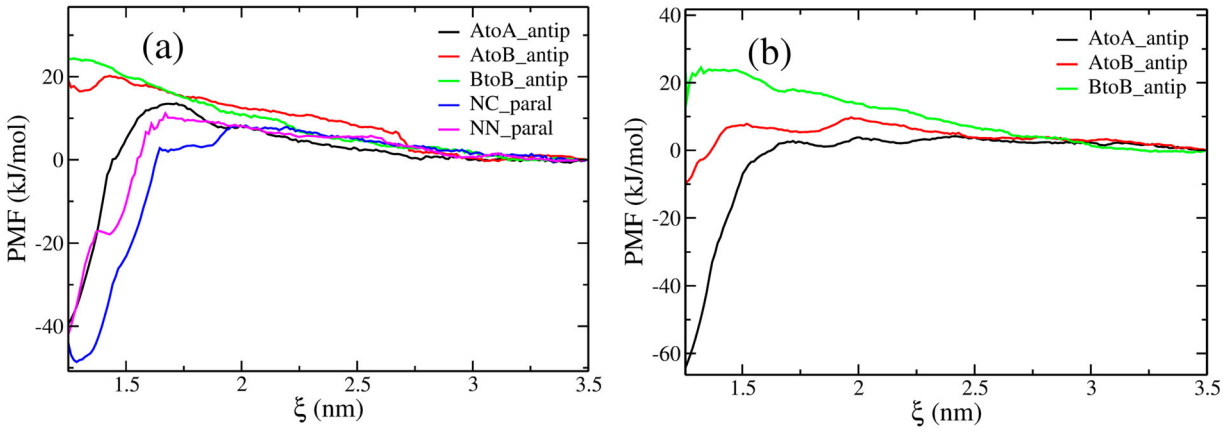

Figure 4. (Colour online) Inter-sheet translational PMFs for KI4K (a) and I4K2 (b).

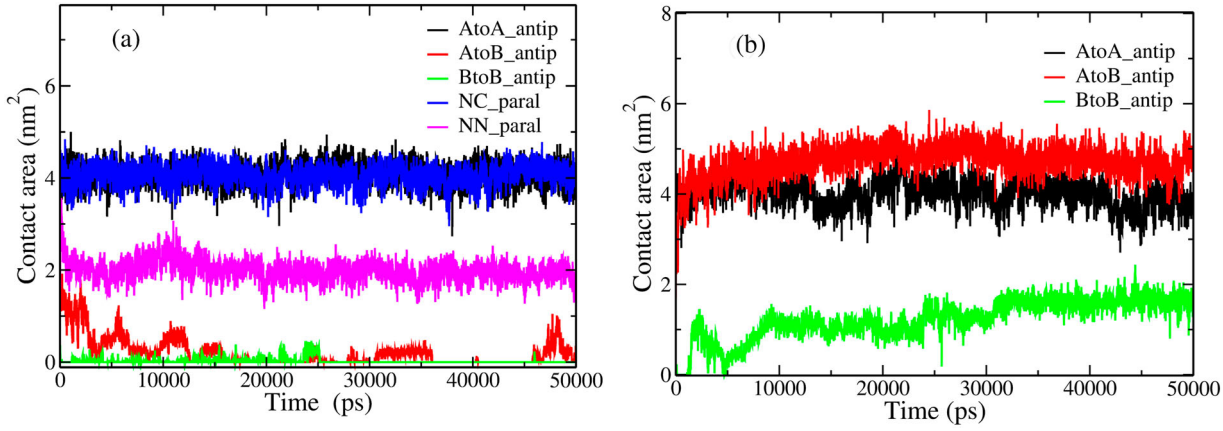

Figure 5. (Colour online) Hydrophobic-hydrophobic-residue contact areas for different inter-sheet structures of KI4K (a) and I4K2 (b).

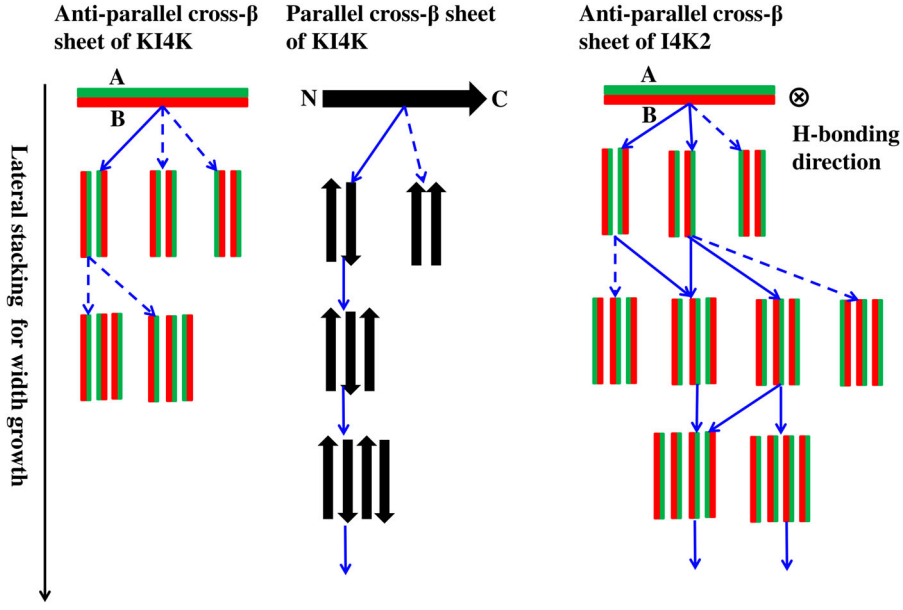

Figure 6. (Colour online) Width growth pathways for KI4K and I4K2. Each bar represents a cross-β sheet, which has three featured directions: the longitudinal direction along the peptide backbone connecting N-terminal and C-terminal, the transversal direction along the peptide side chain, and the vertical direction labelled by '⊗' along the H-bonding direction. In the left and right panels with the antiparallel arrangement, face A is coloured by green and face B is coloured by red. In the middle panel with the parallel arrangement, the black arrow pointing from N-terminal to C-terminal. The blue arrow indicates the direction of a new cross-β sheet stacking on the existing nanostructure with stable stacking patterns marked by solid lines and unstable ones marked by dashed lines.

Table 2. Parameters acquired in the simplified model for KI4K and I4K2.

	k_t	k_b	σ	θ_0	D_0	h_0
KI4K	4.28	2.14	0.3	0.29	0.45	1.2
I4K2	13.6	6.8	0.075	0.33	0.48	1.2

angles θ_0 between neighbouring peptides are the average values of the twisting angles shown in Figure 2(F). The distances between intra-sheet neighbouring peptides D_0 are set to be the valley positions of the PMFs drawn in Figure 2(E). The distances of inter-sheet neighbouring peptides h_0 are the valley positions of PMFs in Figure 4. Unlike the conformation parameters, the strengths of interactions cannot be directly determined from the PMFs due to the harmonic approximation adopted in the simplified model. Among the PMFs in Figures 2(A,B,E) and 4, only the potential wells of PMFs in Figure 2 (A,B) are fitted with the harmonic function to determine the twisting strength k_t. The stretching strength k_b is set to one half of the twisting strength k_t. The inter-sheet energy constant σ for I4K2 is determined according to $\sigma = (1/20)k_t\theta_0^2$. Because the associated energy of the inter-sheet structure for the NC_paral mode of KI4K is about four times of that for the Ato-B_antip mode of I4K2, the inter-sheet energy constant for KI4K is set to be four times of that for I4K2.

The simulation results with the simplified model for KI4K and I4K2 are shown in Figure 7(a), which qualitatively confirm the experimental observation that the morphologies self-assembled by KI4K are apparently wider than I4K2 and tend to be tube-like rather than a twisted tape with a single cross-β sheet. Moreover, the time evolution of the energy and the number of cross-β sheets of the KI4K nanostructure shown in Figure S10 indicate that the outmost cross-β sheet with a higher elastic energy drives the morphological transformation.

To understand the effects of microscopic intermolecular interactions on the self-assembled morphology, three series of simulations are conducted for I4K2: in the first one, only the strength of the intra-sheet interaction k_t decreases; in the second one, only the strength of the inter-sheet interaction σ increases; in the third one, only the twisting degree of intra-sheet θ_0 decreases. The final morphologies in all the simulations are shown in Figure 7(b–d), respectively, and the time evolutions of morphological transformations of different structures are shown in Figures S11–S15. In agreement with the elastic theory, decrease of either the intra-sheet interaction or the twisting degree can promote the width growth, as shown in Figure 7(b,d). On the other hand, increasing the inter-sheet interaction can promote the width growth, as shown in Figure 7(c). Furthermore, other morphologies observed in experiments such as fibrils, twisted ribbons, and nanobelts can also be found for nanostructures with different widths, indicating that our simplified model is not only consistent with the shape selection rule imposed in the original elastic theory, but also enriches the number of objected shapes.

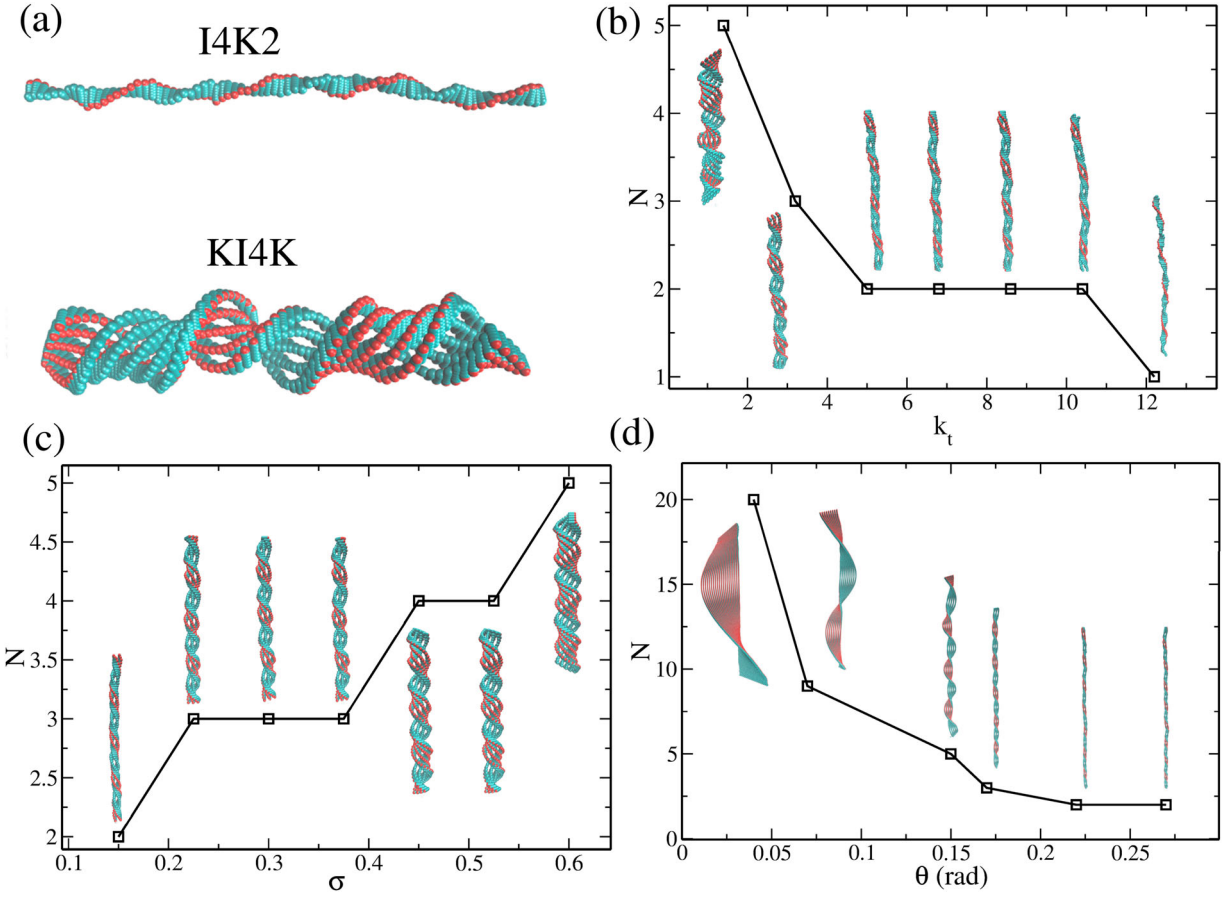

Figure 7. (Colour online) Morphologies and numbers of cross-β sheets given by the simplified model with varied parameters. (a) The self-assembled morphologies of I4K2 and KI4K. (b–d) The I4K2 results with varied intra-sheet interaction, inter-sheet interaction, or twisting degree, respectively.

4. Conclusions

In this work, we propose a multiscale computational approach combining an elastic theory and multiscale simulation techniques to unravel the molecular mechanism of nanostructures with different morphologies formed by peptide self-assembly. Enlightened by the hierarchical model for fibrils proposed by Aggeli et al. [36,37] we first derive a quantitative relation between the nanostructure width and the intermolecular interactions of the hierarchical structures at the molecular level. By considering the balance between the energy cost and the energy gain of the outmost cross-β sheet, our theoretical results demonstrate that the strong inter-sheet attraction, but not the large twisting degree and strong intra-sheet attraction, promotes lateral stacking along the side-chain direction. Furthermore, the intermolecular interactions and underlying molecular structures of the nanostructures can be systematically determined according to the stability and thermodynamics of intra-sheet and inter-sheet structures in all-atom MD simulations. Finally, the simplified model developed in our previous work with its parameters determined from the all-atom MD simulations can bridge the gap between the simulation results at the molecular level and at the mesoscopic level. The simulation results of the simplified model discover not only the relation between the width of the self-assembled nanostructure and the intermolecular interactions, but also the qualitative relation between the width and the nanostructural morphology.

The multiscale computational methods applied to the KI4K and I4K2 systems provide a thorough understanding of the morphological difference between the self-assembled nanostructures of KI4K and I4K2 at the molecular level. The nanostructures of KI4K are formed by lateral stacking of the parallel cross-β sheets with the N side close to the C side of the neighbouring sheet (NC_paral), but those of I4K2 are formed by lateral stacking of antiparallel cross-β sheets with face A close to face B (AtoB_antip). The twisting degree and strength of the intra-sheet structure of parallel cross-β sheet of KI4K are smaller than those of I4K2, but the strength of inter-sheet structure of KI4K with the NC_paral mode is stronger than that of I4K2 with the AtoB_antip mode. Both the intra-sheet and inter-sheet results facilitate the larger width of the nanostructures formed by KI4K than by I4K2. The simulations with the simplified model indicate that KI4K tends to form a tube-like structure while I4K2 tends to form a twisted tape, which is consistent with experimental observations. Since hierarchical structures are common in nanostructures self-assembled by short peptides, the developed multiscale computational approach can be a systematic method for predicting the self-assembled nanostructural morphology solely based on peptide molecular structure, and thus designing short peptides targeting on designated nanostructures.

Acknowledgement

The computations of this work were conducted on the HPC cluster of ITP-CAS.

Disclosure statement

No potential conflict of interest was reported by the author(s).

Funding

This work was supported by the Strategic Priority Research Program of Chinese Academy of Sciences (grant number XDA17010504), the National Natural Science Foundation of China (grant numbers 11504431 and 11947302), and the CAS Biophysics Interdisciplinary Innovation Team Project (grant number 2060299).

ORCID

Yanting Wang http://orcid.org/0000-0002-0474-4790

References

[1] Wang ZG, Ding BQ. Engineering DNA self-assemblies as templates for functional nanostructures. Acc Chem Res. 2014;47(6):1654–1662.
[2] De Santis E, Ryadnov MG. Peptide self-assembly for nanomaterials: the old new kid on the block. Chem Soc Rev. 2015;44(22):8288–8300.
[3] Grabow WW, Jaeger L. RNA self-assembly and RNA nanotechnology. Acc Chem Res. 2014;47(6):1871–1880.
[4] Yan XH, Cui Y, He Q, et al. Reversible transitions between peptide nanotubes and vesicle-like structures including theoretical modeling studies. Chem Eur J. 2008;14(19):5974–5980.
[5] Cui H, Muraoka T, Cheetham AG, et al. Self-assembly of giant peptide nanobelts. Nano Lett. 2009;9(3):945–951.
[6] Adamcik J, Castelletto V, Bolisetty S, et al. Direct observation of time-resolved polymorphic states in the self-assembly of end-capped heptapeptides. Angew Chem Int Ed. 2011;50(24):5495–5498.
[7] Morris KL, Zibaee S, Chen L, et al. The structure of cross-beta tapes and tubes formed by an octapeptide, αSβ1. Angew Chem Int Ed. 2013;52(8):2279–2283.
[8] Knowles TPJ, Buehler MJ. Nanomechanics of functional and pathological amyloid materials. Nat Nanotechnol. 2011;6(8):469–479.
[9] Castelletto V, Hamley IW, Cenker C, et al. Influence of salt on the self-assembly of two model amyloid heptapeptides. J Phys Chem B. 2010;114(23):8002–8008.
[10] Hamley IW, Nutt DR, Brown GD, et al. Influence of the solvent on the self-assembly of a modified amyloid beta peptide fragment. II. NMR and computer simulation investigation. J Phys Chem B. 2010;114(2):940–951.
[11] Zhao YR, Wang JQ, Deng L, et al. Tuning the self-assembly of short peptides via sequence variations. Langmuir. 2013;29(44):13457–13464.
[12] Zhao YR, Deng L, Wang JQ, et al. Solvent controlled structural transition of KI4K self-assemblies: from nanotubes to nanofibrils. Langmuir. 2015;31(47):12975–12983.
[13] Pappas CG, Shafi R, Sasselli IR, et al. Dynamic peptide libraries for the discovery of supramolecular nanomaterials. Nat Nanotechnol. 2016;11(11):960–967.
[14] Knowles TP, Fitzpatrick AW, Meehan S, et al. Role of intermolecular forces in defining material properties of protein nanofibrils. Science. 2007;318(5858):1900–1903.
[15] Fitzpatrick AWP, Debelouchina GT, Bayro MJ, et al. Atomic structure and hierarchical assembly of a cross-beta amyloid fibril. Proc Natl Acad Sci USA. 2013;110(14):5468–5473.
[16] Colletier JP, Laganowsky A, Landau M, et al. Molecular basis for amyloid-beta polymorphism. Proc Natl Acad Sci USA. 2011;108(41):16938–16943.
[17] Nelson R, Sawaya MR, Balbirnie M, et al. Structure of the cross-beta spine of amyloid-like fibrils. Nature. 2005;435(7043):773–778.
[18] Sawaya MR, Sambashivan S, Nelson R, et al. Atomic structures of amyloid cross-beta spines reveal varied steric zippers. Nature. 2007;447(7143):453–457.
[19] Fitzpatrick AWP, Vanacore GM, Zewail AH. Nanomechanics and intermolecular forces of amyloid revealed by four-dimensional electron microscopy. Proc Natl Acad Sci USA. 2015;112(11):3380–3385.
[20] Schmidt A, Annamalai K, Schmidt M, et al. Cryo-EM reveals the steric zipper structure of a light chain-derived amyloid fibril. Proc Natl Acad Sci USA. 2016;113(22):6200–6205.

[21] Mehta AK, Lu K, Childers WS, et al. Facial symmetry in protein self-assembly. J Am Chem Soc. 2008;130(30):9829–9835.
[22] Paravastu AK, Leapman RD, Yau WM, et al. Molecular structural basis for polymorphism in Alzheimer's beta-amyloid fibrils. Proc Natl Acad Sci USA. 2008;105(47):18349–18354.
[23] Petkova AT, Leapman RD, Guo ZH, et al. Self-propagating, molecular-level polymorphism in Alzheimer's beta-amyloid fibrils. Science. 2005;307(5707):262–265.
[24] Pashuck ET, Stupp SI. Direct observation of morphological tranformation from twisted ribbons into helical ribbons. J Am Chem Soc. 2010;132(26):8819–8821.
[25] Lee HY, Oh H, Lee JH, et al. Shedding light on helical microtubules: real-time observations of microtubule self-assembly by light microscopy. J Am Chem Soc. 2012;134(35):14375–14381.
[26] Thirumalai D, Reddy G, Straub JE. Role of water in protein aggregation and amyloid polymorphism. Acc Chem Res. 2012;45(1):83–92.
[27] Nguyent P, Derreumaux P. Understanding amyloid fibril nucleation and a beta oligomer/drug interactions from computer simulations. Acc Chem Res. 2014;47(2):603–611.
[28] Morriss-Andrews A, Shea JE. computational studies of protein aggregation: methods and applications. Annu Rev Phys Chem. 2015;66(1):643–666.
[29] Gnanakaran S, Nussinov R, Garcia AE. atomic-level description of amyloid beta-dimer formation. J Am Chem Soc. 2006;128(7):2158–2159.
[30] Wei GH, Jewett AI, Shea JE. Structural diversity of dimers of the Alzheimer amyloid-beta(25-35) peptide and polymorphism of the resulting fibrils. Phys Chem Chem Phys. 2010;12(14):3622–3629.
[31] Deng L, Zhou P, Zhao YR, et al. Molecular origin of the self-assembled morphological difference caused by varying the order of charged residues in short peptides. J Phys Chem B. 2014;118(43):12501–12510.
[32] Mondal J, Yethiraj A. Driving force for the association of amphiphilic molecules. J Phys Chem Lett. 2011;2(19):2391–2395.
[33] Ndlovu H, Ashcroft AE, Radford SE, et al. Effect of sequence variation on the mechanical response of amyloid fibrils probed by steered molecular dynamics simulation. Biophys J. 2012;102(3):587–596.
[34] Marrink SJ, Tieleman DP. Perspective on the martini model. Chem Soc Rev. 2013;42(16):6801–6822.
[35] Guo C, Luo Y, Zhou RH, et al. Probing the self-assembly mechanism of diphenylalanine-based peptide nanovesicles and nanotubes. ACS Nano. 2012;6(5):3907–3918.
[36] Nyrkova I, Semenov AN, Aggeli A, et al. Fibril stability in solutions of twisted-sheet peptides: a new kind of micellization in chiral systems. Eur Phys J B. 2000;17(3):481–497.
[37] Aggeli A, Nyrkova IA, Bell M, et al. Hierarchical self-assembly of chiral rod-like molecules as a model for peptide beta-sheet tapes, ribbons, fibrils, and fibers. Proc Natl Acad Sci USA. 2001;98(21):11857–11862.
[38] Deng L, Zhao YR, Xu H, et al. Intrinsic defect formation in peptide self-assembly. Appl Phys Lett. 2015;107(4):043701.
[39] Jorgensen WL, Maxwell DS, Titado-Rives J. Development and testing of the opls all-atom force field on conformational energetics and properties of organic liquids. J Am Chem Soc. 1996;118(45):11225–11236.
[40] Jorgensen WL, William L, Chandrasekhar J, et al. Comparison of simple potential functions for simulating liquid water. J Chem Phys. 1983;79(2):926–935.
[41] DeLano WL. The PyMOL molecular graphics system. Palo Alto (CA): DeLano Scientific LLC; 2002.
[42] Van der Spoel D, Lindahl E, Hess B, et al. GROMACS: fast, flexible, and free. J Comput Chem. 2005;26(16):1701–1718.
[43] Darden T, York D, Pedersen L. Particle mesh Ewald: An N·log(N) method for Ewald sums in large systems. J Chem Phys. 1993;98(12):10089–10092.
[44] Nose S. A molecular dynamics method for simulations in the canonical ensemble. Mol Phys. 1984;52(2):255–268.
[45] Parrinello M, Rahman A. Polymorphic transitions in single crystals: a new molecular dynamics method. J Appl Phys. 1981;52(12):7182–7190.
[46] Kutzner C, Czub J, Grubmuller H. Keep it flexible: driving macromolecular rotary motions in atomistic simulations with GROMACS. J Chem Theor Comput. 2011;7(5):1381–1393.
[47] Kumar S, Bouzida D, Swendsen RH, et al. The weighted histogram analysis method for free energy calculations on biomolecules. I. The method. J Comb Chem. 1992;13(8):1011–1021.
[48] Hukushima K, Nemoto K. Exchange Monte Carlo method and application to spin glass simulations. J Phys Soc Jpn. 1996;65(6):1604–1608.
[49] Sugita Y, Okamoto Y. Replica-exchange molecular dynamics method for protein folding. Chem Phys Lett. 1999;314(1):142–151.
[50] Chong SH, Ham S. Impact of chemical heterogeneity on protein self-assembly in water. Proc Natl Acad Sci USA. 2012;109(20):7636–7641.